# Brownian heat engine with active reservoirs

Jae Sung Lee, Jong-Min Park, and Hyunggyu Park*
*School of Physics and Quantum Universe Center, Korea Institute for Advanced Study, Seoul 02455, Korea*

(Received 11 January 2020; accepted 18 August 2020; published 9 September 2020)

Microorganisms such as bacteria are active matter which consume chemical energy and generate their unique run-and-tumble motion. A swarm of such microorganisms provide a nonequilibrium active environment whose noise characteristics are different from those of thermal equilibrium reservoirs. One important difference is a finite persistence time, which is considerably large compared to that of the equilibrium noise, that is, the active noise is colored. Here we study a mesoscopic energy-harvesting device (engine) with active reservoirs harnessing this noise nature. For an exactly solvable linear model, we show that the performance from the active environment can surpass that from the equilibrium environment. Furthermore, we propose a proper definition of the active-reservoir temperature and show that the engine efficiency can overcome the conventional Carnot bound, thus the power-efficiency trade-off constraint is released. We also show that the efficiency at the maximum power can surpass the Curzon-Ahlborn efficiency. This remarkable enhancement originates from the extra unconventional entropy production beyond the conventional Clausius entropy production, due to the non-Markovian nature of the active reservoirs. Interestingly, the supremacy of the active engine critically depends on the timescale symmetry of two active reservoirs.

DOI: 10.1103/PhysRevE.102.032116

## I. INTRODUCTION

Mounting social need on sustainable development has attracted great attention on energy harvesting techniques, by which useful energy is extracted from surrounding environments, in both scientific and engineering societies [1–3]. Typical examples are thermoelectric devices using a temperature gradient [4], photovoltaic devices using sunlight [5], and piezoelectric devices using ambient pressure [6]. A major challenging issue on these studies is achieving a high efficiency as well as a high energy or power production. When a device works in an equilibrium environment, the efficiency is bound by the thermodynamic second law; for example, the efficiency of thermoelectric devices cannot surpass the Carnot efficiency.

How, then, is the efficiency affected by replacing the environment with nonequilibrium reservoirs? One might think that the efficiency would be reduced with nonequilibrium reservoirs as the efficiency usually diminishes with irreversibility. However, this is not always true: It was already reported that the efficiency of a quantum heat engine can surpass the conventional Carnot limit with nonequilibrium *squeezed* reservoirs [7–9]. In classical systems, it was experimentally shown that the efficiency of a Stirling engine working in a bacterial bath can overcome its maximum efficiency obtained by a quasistatic operation in equilibrium reservoirs [10,11]. In addition, there are also a few examples where the efficiency increases with the irreversibility in well-manipulated ways [12–14]. However, a systematic study on the efficiency bound of engines working in nonequilibrium environments has rarely been done, partly because its theoretical manipulation is not straightforward as in the equilibrium cases.

In this work, we study the efficiency and the power of an energy-harvesting device extracting energy from nonequilibrium *active* reservoirs. To be specific, we consider an overdamped Brownian motion of passive particles composing of the engine with equilibrium baths and/or bacterial active baths. A bacterial bath is known to be well described by the colored noise with a finite persistence timescale [15–20]. In the case with the active baths, we demonstrate rigorously that (i) the efficiency can surpass the standard Carnot limit, thus the conventional power-efficiency trade-off relation [21–23] does not hold, and (ii) the efficiency at the maximum power (EMP) can overcome the Curzon-Ahlborn (CA) efficiency [24].

This enhancement can be understood in the entropic perspective; while the total entropy production (EP) is still nonnegative, the existence of an extra unconventional EP can make the Clausius EP negative [25–29]. We emphasize that the thermodynamic second law is still valid with the proper inclusion of the unconventional EP for the complete thermodynamic accounting, which is similar to the presence of the extra mutual information EP in the famous Maxwell's demon problem [30]. We also find that the supremacy of the active engine is achieved when the timescales of the two active baths are different from each other. Our results clearly show that the environmental noise from active particles can be used as a valuable energy source for a energy-harvesting device with better performance.

## II. ENGINE WITH EQUILIBRIUM RESERVOIRS

We first revisit the simple linear Brownian engine model with equilibrium reservoirs in the overdamped limit [31,32]. Suppose that there are two particles (particle 1 and 2), each of which moves in a one-dimensional space and is immersed

*hgpark@kias.re.kr

 

in a heat reservoir with temperature $T_i$ $(i = 1, 2)$. Their positions are denoted by $x_1$ and $x_2$ and $\Phi = \Phi(x_1, x_2)$ is a given potential. The motions of these particles are described by the following equations:

$$\gamma_i \dot{x}_i = -\partial_{x_i}\Phi + f_i^{\rm nc} + \sqrt{2k_B\gamma_i T_i}\xi_i, \tag{1}$$

where $\gamma_i$ is a dissipation coefficient, $f_i^{\rm nc}$ is an external nonconservative force, and $k_B$ is the Boltzmann constant, which will be set to 1 in the following discussion. $\xi_i$ is a Gaussian white noise satisfying $\langle \xi_i(t)\rangle = 0$ and $\langle \xi_i(t)\xi_j(t')\rangle = \delta_{ij}\delta(t-t')$. In this model, the harmonic potential and the linear nonconservative force are taken for analytic treatments [32–34] as

$$\Phi = \frac{k}{2}\left(x_1^2 + x_2^2\right), \quad \left(f_1^{\rm nc}, f_2^{\rm nc}\right) = (\epsilon x_2, \delta x_1). \tag{2}$$

Note that the Brownian gyrator [35] has a similar structure, which was experimentally realized recently [36].

From Eq. (1), the thermodynamic first law can be written as

$$\dot{Q}_i = \dot{E}_i + \dot{W}_i, \tag{3}$$

where $\dot{E}_i = \dot{x}_i\partial_{x_i}\Phi$ is the rate of the internal energy change of a particle $i$, $\dot{W}_i = -f_i^{\rm nc}\dot{x}_i$ is the work extraction rate due to the external force $f_i^{\rm nc}$, and $\dot{Q}_i = \dot{x}_i \circ (-\gamma_i\dot{x}_i + \sqrt{2\gamma_i T_i}\xi_i)$ is the heat current from the bath $i$ with the Stratonovich multiplication denoted by $\circ$ [37]. In the steady state, $\langle \dot{Q}_i\rangle_s = \langle \dot{W}_i\rangle_s$ as $\langle \dot{E}_i\rangle_s = 0$, where $\langle\cdots\rangle_s$ denotes the steady-state average. Therefore, $\langle \dot{Q}_1\rangle_s = -\epsilon\langle x_2\dot{x}_1\rangle_s$ and $\langle \dot{Q}_2\rangle_s = -\delta\langle x_1\dot{x}_2\rangle_s$. The total work rate (power) is $\langle \dot{W}\rangle_s = \langle \dot{W}_1\rangle_s + \langle \dot{W}_2\rangle_s = (\epsilon - \delta)\langle x_1\dot{x}_2\rangle_s$, where the second equality comes from the fact $\frac{d}{dt}\langle x_1x_2\rangle_s = \langle \dot{x}_1x_2\rangle_s + \langle x_1\dot{x}_2\rangle_s = 0$.

For $T_1 > T_2$, the efficiency $\eta$ is given by the ratio between $\langle \dot{W}\rangle_s$ and $\langle \dot{Q}_1\rangle_s$ as

$$\eta = \frac{\langle \dot{W}\rangle_s}{\langle \dot{Q}_1\rangle_s} = 1 - \frac{\delta}{\epsilon}. \tag{4}$$

Requiring the work extraction $\langle \dot{W}\rangle_s = (\epsilon - \delta)\langle x_1\dot{x}_2\rangle_s \geqslant 0$ with

$$\langle x_1\dot{x}_2\rangle_s = \frac{T_1\delta - T_2\epsilon}{k(\gamma_1 + \gamma_2)}, \tag{5}$$

we find the constraint $T_2/T_1 \leqslant \delta/\epsilon \leqslant 1$, leading to the famous Carnot bound as

$$0 \leqslant \eta \leqslant 1 - \frac{T_2}{T_1} \equiv \eta_C, \tag{6}$$

where $\eta_C$ is the Carnot efficiency. As expected from the power-efficiency trade-off relation, the power $\langle \dot{W}\rangle_s$ vanishes at $\eta = \eta_C$ [21–23]. In addition, we need the stability condition for the existence of the steady state, which turns out to be

$$\delta\epsilon \equiv K < k^2. \tag{7}$$

Derivations of Eqs. (5) and (7) are presented in Appendix A1.

Figure 1(a) shows the engine area satisfying the above two constraints (6) and (7) with $\gamma_1 = \gamma_2 = 1$, $k = 2$, $T_1 = 2$, and $T_2 = 1$. In Fig. 1(b), we plot the normalized efficiency and power as $\tilde{\eta} \equiv \eta/\eta_C$ and $\tilde{P} \equiv \langle \dot{W}\rangle_s/P_{\rm eq}^{\rm max}$ along the line from $\epsilon_1$ to $\epsilon_2$ of Fig. 1(a) at fixed $\delta = 0.8$, where $P_{\rm eq}^{\rm max}$ is the maximum power in equilibrium baths defined as Eq. (8). Note that the solid curves and data points of Fig. 1 are analytic curves and numerical simulation results, respectively. All numerical data are obtained by integrating the equations of motion of Eq. (1) and averaging over $2 \times 10^6$ samples in the steady state.

We also calculate the efficiency at the maximum power (EMP) $\eta_{\rm EMP}$. Along the curve with fixed $K$ $(0 \leqslant K \leqslant k^2)$, the local maximum power is obtained at $\delta_m = \sqrt{T_2/T_1}\epsilon_m$ with the efficiency $\eta_m$ identical to the CA efficiency $\eta_{\rm CA}$ [24] and the power given by $\langle \dot{W}\rangle_s^m = KT_1\eta_{\rm CA}^2/k(\gamma_1 + \gamma_2)$. The global power maximum is achieved at $K = k^2$, and thus we obtain

$$\eta_{\rm EMP} = 1 - \sqrt{\frac{T_2}{T_1}} \equiv \eta_{\rm CA} \quad \text{and} \quad P_{\rm eq}^{\rm max} \equiv \frac{kT_1\eta_{\rm CA}^2}{\gamma_1 + \gamma_2}. \tag{8}$$

Figure 1(c) shows the plots of $\tilde{\eta}_m \equiv \eta_m/\eta_{\rm CA}$ and $\tilde{P}_m \equiv \langle \dot{W}\rangle_s^m/P_{\rm eq}^{\rm max}$ against $K$.

## III. ENGINE WITH ACTIVE RESERVOIRS

Now we replace equilibrium reservoirs with bacterial active baths. The equations of motion are given as

$$\gamma_i \dot{x}_i = -\partial_{x_i}\Phi + f_i^{\rm nc} + \zeta_i. \tag{9}$$

Here $\zeta_i$ is a Gaussian colored noise satisfying $\langle \zeta_i(t)\zeta_j(t')\rangle = D_i\delta_{ij}e^{-|t-t'|/\tau_i}/\tau_i$, where $D_i$ is the noise strength and $\tau_i$ is the persistence timescale of noise $\zeta_i$ [15–20]. The finite persistent time originates from collisions of a passive particle with bacteria with directional persistence. In the $\tau_i \to 0$ limit, the active bath becomes identical to the equilibrium bath with the temperature $T_i = D_i/\gamma_i$. The Ornstein-Uhlenbeck process (OUP) provides one of the simplest ways to describe the evolution of $\zeta_i$ [37]:

$$\tau_i\dot{\zeta}_i = -\zeta_i + \sqrt{2D_i}\xi_i, \tag{10}$$

where $\xi_i$ is a Gaussian white noise as seen in Eq. (1). Together with Eq. (9), this process with linear forces like in Eq. (2) is called the active OUP (AOUP) [20,38–40]. We remark that a non-Gaussian nature of the colored noise was observed experimentally in a low-concentration bacterial bath [17]. However, our results in the following can also apply to a non-Gaussian case because the work and heat current in the linear-force system do not depend on the higher-order moments of the noise except for the second-order one [11].

Before investigating the AOUP engine, we first consider passive particles trapped in a harmonic potential in Eq. (2) without a nonconservative force ($f_i^{\rm nc} = 0$), in contact with the active reservoir. From its steady-state distribution, we can unambiguously define the appropriate *effective* temperature of the active reservoir as follows. It is straightforward (see Appendix A2) to derive the steady-state distribution which is Boltzmannlike in this case as

$$P(x_1, x_2) = \prod_{i=1}^{2}\sqrt{\frac{k}{2\pi T_i^e}}e^{-\frac{kx_i^2}{2T_i^e}}, \tag{11}$$

where the effective temperature $T_i^e \equiv D_i/\Gamma_i$ with $\Gamma_i = \gamma_i + k\tau_i$. Note that $T_i^e \leqslant D_i/\gamma_i = T_i$ and depends not only on the persistent time $\tau_i$ but also on the stiffness $k$ of the harmonic potential. It is not surprising to see the effectively lower temperature because the persistence reduces the stochasticity.

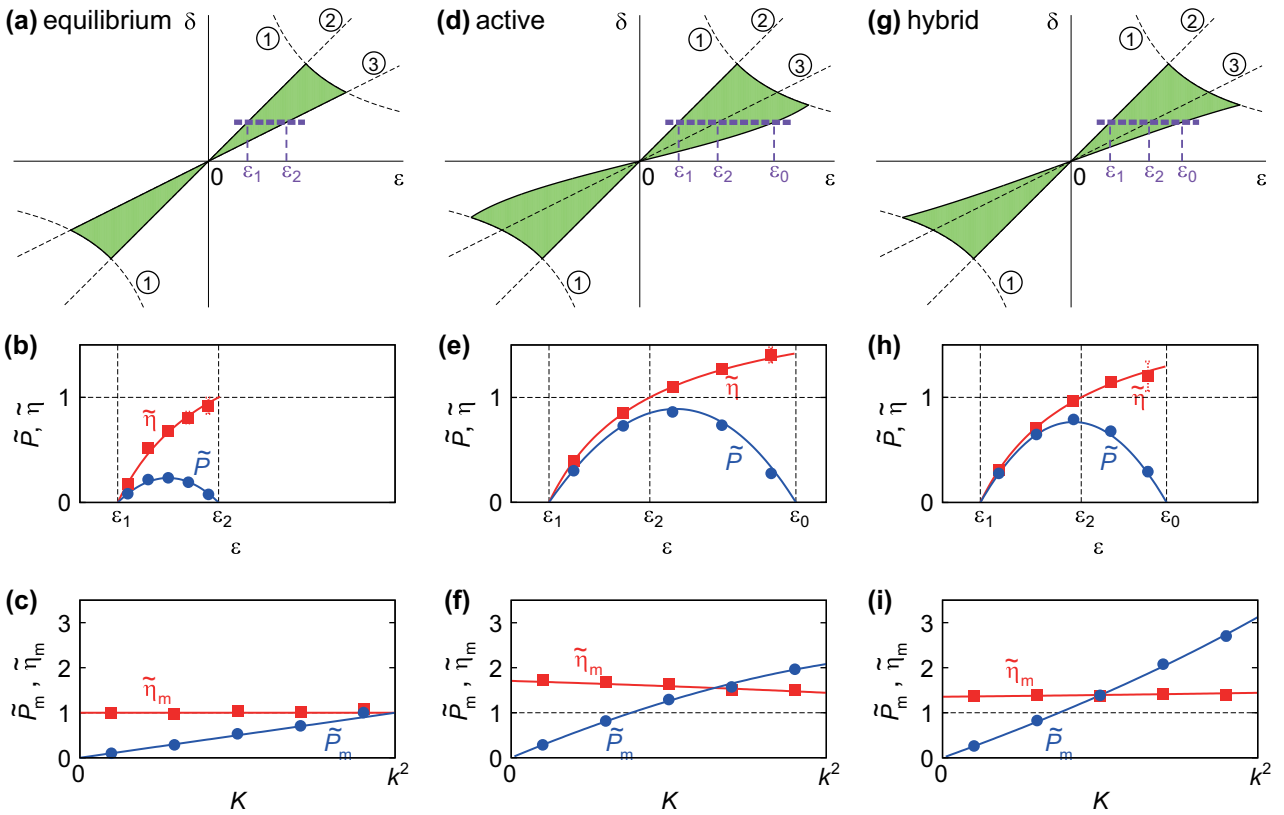


FIG. 1. Performance of the engine in various environments. Shaded areas in panels (a), (d), and (g) denote the areas in which the device works as a stable and useful engine for equilibrium, active, and hybrid reservoirs, respectively. ①, ②, and ③ denote the curves $\epsilon\delta = k^2$, $\delta = \epsilon$, and $\delta = \epsilon T_2/T_1$ or $\delta = \epsilon T_2^e/T_1^e$, respectively. Panels (b), (e), and (h) show the plots of $\tilde{\eta} \equiv \eta/\eta_C$ or $\tilde{\eta} \equiv \eta/\eta_C^e$ and $\tilde{P} \equiv \langle \dot{W} \rangle_s / P_{\rm eq}^{\rm max}$ along the thick dashed line of panels (a), (d), and (g) from $\epsilon_1$ to $\epsilon_2$ or $\epsilon_0$ at fixed $\delta = 0.8$, respectively. The efficiency for the active and the hybrid baths can surpass the effective Carnot efficiency $\eta_C^e$ while the efficiency of the equilibrium bath is bounded by the conventional $\eta_C$. Solid curves and data points indicate analytic and numerical results, respectively. Panels (c), (f), and (i) show the plots of $\tilde{\eta}_m \equiv \eta_m/\eta_{\rm CA}$ or $\tilde{\eta}_m \equiv \eta_m/\eta_{\rm CA}^e$ and $\tilde{P}_m \equiv \langle \dot{W} \rangle_s^m / P_{\rm eq}^{\rm max}$ against $K(=\delta\epsilon)$. The EMP for the active and the hybrid bath surpass $\eta_{\rm CA}^e$. The maximum power also become larger for the active and the hybrid baths than that for the equilibrium bath.

The energy conservation yields again Eq. (3) where the heat current from the active bath $i$ is given by $\dot{Q}_i = \dot{x}_i \circ (-\gamma_i \dot{x}_i + \zeta_i)$. In the steady state for the AOUP engine, we get the same form as before for the heats and power such as $\langle \dot{Q}_1 \rangle_s = \langle \dot{W}_1 \rangle_s = \epsilon \langle x_1 \dot{x}_2 \rangle_s$ and $\langle \dot{W} \rangle_s = (\epsilon - \delta)\langle x_1 \dot{x}_2 \rangle_s$. The standard calculation of the multivariate OUP [37] by treating the colored noise $\zeta_i$ as a state variable yields (see Appendix A3)

$$\langle x_1 \dot{x}_2 \rangle_s = \frac{1}{k(\gamma_1 + \gamma_2)} \left[ \frac{T_1^e \delta}{\mathcal{A}_K} - \frac{T_2^e \epsilon}{\mathcal{B}_K} \right] \quad \text{with } K = \delta\epsilon, \tag{12}$$

where

$$\mathcal{A}_K = 1 + \frac{k\gamma_1\tau_1}{\gamma_2\Gamma_1} + \frac{(k^2 - K)\tau_1^2}{\gamma_2\Gamma_1},$$
$$\mathcal{B}_K = 1 + \frac{k\gamma_2\tau_2}{\gamma_1\Gamma_2} + \frac{(k^2 - K)\tau_2^2}{\gamma_1\Gamma_2}. \tag{13}$$

We find the same stability condition ($K < k^2$, see Appendix A3) and thus $\mathcal{A}_K \geqslant 1$ and $\mathcal{B}_K \geqslant 1$ in the stable region.

In this study, we define the efficiency of an active engine (or hybrid engine in the next section) as the conventional one for a passive engine, i.e., a fraction of the extracted work from the absorbed energy from the *hot* reservoir. More discussion on the definition of the efficiency for an active engine is presented at the end of this section. With this definition, we find the efficiency bound from the engine condition as

$$0 \leqslant \eta = 1 - \frac{\delta}{\epsilon} \leqslant 1 - \frac{T_2^e \mathcal{A}_K}{T_1^e \mathcal{B}_K} \equiv \eta_C^a, \tag{14}$$

where $\eta_C^a$ is the maximum efficiency for the AOUP engine. It is remarkable to see that $\eta_C^a$ can exceed the effective Carnot efficiency $\eta_C^e = 1 - T_2^e/T_1^e$ when the modification factor $\mathcal{M}_K \equiv \mathcal{B}_K/\mathcal{A}_K > 1$. The modification factor $\mathcal{M}_K$ is maximized and reaches $1 + k\tau_2/\gamma_1$ in the limits of $\tau_1/\tau_2 \to 0$ and $K \to 0$.

The case with the timescale symmetry ($\tau_1 = \tau_2$ and $\gamma_1 = \gamma_2$) is special. We get $\mathcal{M}_K = 1$ and $T_2^e/T_1^e = T_2/T_1$, and thus $\eta_C^a = 1 - T_2/T_1 = \eta_C$; no effect on the efficiency but the power is reduced by a factor of $\mathcal{A}_K(1 + k\tau_1/\gamma_1) \geqslant 1$. Therefore, the breaking of the timescale symmetry is crucial in enhancing the engine performance. Similar phenomena were found recently in some quantum engines [41,42], where the quantumness disappears with the symmetry.

Furthermore, we can see that the active engine can do work with two active reservoirs with the same effective temperatures but with different persistence times. This also manifests

that the active reservoir should be characterized not only by its effective temperature but also by its persistent time. More remarkably, the heat flows can be reversed ($\langle \dot{Q}_1 \rangle_s < 0$, $\langle \dot{Q}_2 \rangle_s > 0$ for $T_1^e \geqslant T_2^e$), still with the positive work extraction $\langle \dot{W} \rangle_s > 0$) when $T_2^e/\mathcal{B}_K > T_1^e/\mathcal{A}_K$ (see detailed discussions in Appendix A3).

To illustrate the enhancement of the active engine performance, we consider a simple case with $\tau_1 = 0$ (high-temperature equilibrium reservoir) and $\tau_2 > 0$ (low-temperature active reservoir). Then it is clear that $\eta_C^a$ is always larger than $\eta_C^e$ as $\mathcal{A}_K = 1$ and $\mathcal{B}_K > 1$. Furthermore, as $T_1^e = T_1$ and $T_2^e = T_2/(1 + k\tau_2/\gamma_2) < T_2$, we find $\eta_C^a > \eta_C^e > \eta_C$. From Eq. (12), we can also easily see that the power is enhanced in this case, compared to the case of both equilibrium reservoirs ($\tau_1 = \tau_2 = 0$).

Figure 1(d) shows the region satisfying the stable and useful engine condition with $\tau_1 = 0$, $\tau_2 = 0.5$, $T_1^e = 2$, and $T_2^e = 1$, which is extended outside of the line of $\delta = (T_2^e/T_1^e)\epsilon$, where the efficiency $\eta$ is larger than $\eta_C^e$. The boundary of the extended region is given by $\langle x_1 \dot{x}_2 \rangle_s = 0$ in Eq. (12); thus in this case, $\delta = [T_2^e/(\mathcal{B}_K T_1^e)]\epsilon$, which is not a straight line because of $K = \delta\epsilon$. In Fig. 1(e), the normalized efficiency and power as $\tilde{\eta} \equiv \eta/\eta_C^e$ and $\tilde{P} \equiv \langle \dot{W} \rangle_s / P_{\rm eq}^{\rm max}$ along the thick dashed line from $\epsilon_1$ to $\epsilon_0$ of Fig. 1(d) are plotted at fixed $\delta = 0.8$, where $\epsilon_0$ is the largest point allowed in the engine region. The efficiency clearly exceeds the effective Carnot efficiency by far and the power is finite even at the effective Carnot efficiency. This shows that the conventional power-efficiency trade-off constraint [21–23] is not valid in the active engine.

We also show that the EMP of this AOUP engine can surpasses the CA efficiency. Along the curve with fixed $K$, the local maximum power is obtained at $\delta_m = \sqrt{T_2^e/(\mathcal{B}_K T_1^e)}\epsilon_m$ with the efficiency and the power

$$\eta_m = 1 - \sqrt{\frac{T_2^e}{\mathcal{B}_K T_1^e}} > \eta_{\rm CA}^e \quad \text{and} \quad \langle \dot{W} \rangle_s^m \equiv \frac{K T_1^e \eta_m^2}{k(\gamma_1 + \gamma_2)}, \tag{15}$$

where $\eta_{\rm CA}^e \equiv 1 - \sqrt{T_2^e/T_1^e}$ is the effective CA efficiency. The global power maximum is achieved at a nontrivial value of $K$ for $0 \leqslant K \leqslant k^2$ and $\eta_{\rm EMP}$ exceeds $\eta_{\rm CA}^e$. Figure 1(f) shows the plots of $\tilde{\eta}_m \equiv \eta_m/\eta_{\rm CA}^e$ and $\tilde{P}_m \equiv \langle \dot{W} \rangle_s^m / P_{\rm eq}^{\rm max}$ against $K$. Note that the dependence of $\eta_C^a$ and $\langle \dot{W} \rangle_s^m$ on general $\tau_1$ and $\tau_2$ is presented in Appendix B.

In the above example, it is easy to understand why the efficiency $\eta$ can be larger than $\eta_C$: This is simply because $T_2^e < T_2$ which provides effectively the bigger temperature gradient. However, there is a nontrivial additional enhancement of the engine performance, which is encoded in the modification factor $\mathcal{M}_K$. In order to understand this remarkable effect, it is useful to resort to a different representation of the equations of motion of the active engine as follows.

It is well known that the AOUP can be mapped on an underdamped Langevin dynamics by introducing an auxiliary velocity $v_i \equiv \dot{x}_i$ and mass $m_i \equiv \gamma_i \tau_i$ as follows [38–40]:

$$\begin{aligned} \dot{x}_1 &= v_1, \quad m_1 \dot{v}_1 = -k x_1 + \epsilon x_2 + \tau_1 \epsilon v_2 - \Gamma_1 v_1 + \sqrt{2D_1}\xi_1, \\ \dot{x}_2 &= v_2, \quad m_2 \dot{v}_2 = -k x_2 + \delta x_1 + \tau_2 \delta v_1 - \Gamma_2 v_2 + \sqrt{2D_2}\xi_2, \end{aligned} \tag{16}$$

which describes the dynamics of a particle in a harmonic trap with the nonconservative force $f_i^{\rm nc}$ and the unusual *non-anti-symmetric* Lorentz-like velocity-dependent force ($\tau_1 \epsilon v_2$, $\tau_2 \delta v_1$) in contact with the equilibrium reservoirs with the temperature $T_i^e = D_i/\Gamma_i$. The standard antisymmetric Lorenz force such as a magnetic force does not do work by itself. However, the non-anti-symmetric Lorentz-like force can do work as well as change the steady-state distribution function in a significant way. Thus, the existence of the velocity-dependent force can promote the work rate as well as the heat rate, which makes it possible to exceed the effective Carnot efficiency. Note that the heat flow from the active reservoir in this representation is given as $\dot{Q}_1^a = v_1 \circ (\tau_1 \epsilon v_2 - \Gamma_1 v_1 + \sqrt{2D_1}\xi_1)$ and similarly for $\dot{Q}_2^a$, of which the steady-state averages are identical to the heat rates $\langle \dot{Q}_1 \rangle_s$ and $\langle \dot{Q}_1 \rangle_s$ calculated previously.

It is also useful to study the EP or irreversibility for the active engine. Some years ago, Zamponi *et al.* showed that the stochastic thermodynamic approach for the EP can be generalized to a non-Markovian process with a memory kernel [25]. Very recently, the EP for the AOUP was explicitly derived using this method, which turns out to be equivalent to the EP obtained for the above auxiliary underdamped dynamics with the *standard* definition of the parity [26,27,38]. Furthermore, the EP calculation method in an underdamped dynamics with general velocity-dependent forces is well documented [28,29]. In this study, we take this latter approach to derive the EP for the AOUP engine exactly and show that the *unconventional* EP term appearing generally with velocity-dependent forces plays a key role, which provides the main source for the efficiency surpassing the Carnot efficiency in the EP perspective (see Appendix C).

Finally, we remark on the efficiency definition for an active engine. The efficiency is a measure for denoting how efficient an engine performance is. Thus, it is usually defined as a fraction of produced work from the total cost. For an equilibrium reservoir, the absorbed heat $Q_1$ is the total cost to maintain the reservoir. For an active reservoir, however, one may consider an additional cost to maintain the nonequilibrium steady state of the reservoir besides $Q_1$. This may be the cost for feeding and growing bacteria. It is difficult, if not impossible at this moment, to systematically estimate this feeding cost in the energy perspective. Nevertheless, this feeding is expected to be not very costly as we can witness in our daily life that many bacteria can proliferate in the water by themselves even without supplying food because microorganisms are everywhere and abundant in nature, especially in biological environments at the cellular level. In this sense, this additional cost may be practically negligible and our definition of the efficiency is useful for the active and hybrid engines. However, in a strict sense, our efficiency is an upper bound without considering this additional cost.

## IV. ENGINE WITH HYBRID RESERVOIRS

Finally, we consider a more realistic *hybrid* engine by adding active particles (bacteria) into equilibrium fluid reservoirs [18–20,27]. Then, the equations of motion are given by

$$\gamma_i \dot{x}_i = -\partial_{x_i}\Phi + f_i^{\rm nc} + \zeta_i + \sqrt{2\gamma_i T_i}\xi_i', \tag{17}$$

where the reservoir noise is composed of two independent noises: a Gaussian white noise $\xi_i'$ with $\langle \xi_i'(t)\xi_j'(t')\rangle = \delta_{ij}\delta(t-t')$ and a Gaussian colored noise $\zeta_i$ with $\langle \zeta_i(t)\zeta_j(t')\rangle = D_i\delta_{ij}e^{-|t-t'|/\tau_i}/\tau_i$. Equation (17) can also describe the dynamics of a self-propelled particle as an engine particle with equilibrium baths [43].

In the steady state, the power and heat rates are expressed in the same form as before, e.g., $\langle \dot{W}\rangle_s = (\epsilon-\delta)\langle x_1\dot{x}_2\rangle_s$. Following the previous calculation procedure, we find (see Appendix A4)

$$\langle x_1\dot{x}_2\rangle_s = \frac{T_1\delta - T_2\epsilon}{k(\gamma_1+\gamma_2)} + \frac{1}{k(\gamma_1+\gamma_2)}\left(\frac{D_1\delta}{\Gamma_1\mathcal{A}_K} - \frac{D_2\epsilon}{\Gamma_2\mathcal{B}_K}\right), \tag{18}$$

which is a simple sum of two currents due to equilibrium noises and active noises. Note that the power can be enhanced (or reduced) by adding the active noise into the high-temperature (low-temperature) reservoir. In Figs. 1(g), 1(h) and 1(i), we plot the engine region, the power, and the efficiency with the parameters $\tau_1 = 0.5$, $\tau_2 = 0$, $T_1 = 2$, $T_2 = 1$ $D_1 = 3$, and $D_2 = 0$. We also obtain the effective temperature of the hybrid reservoir as $T_i^e = T_i + D_i/\Gamma_i$ (see Appendix A2), and then the engine condition yields

$$0 \leqslant \eta \leqslant 1 - \frac{T_2^e + T_2(\mathcal{B}_K-1)}{T_1^e + T_1(\mathcal{A}_K-1)}\left(\frac{\mathcal{A}_K}{\mathcal{B}_K}\right) \equiv \eta_C^{\text{hybrid}}, \tag{19}$$

with the maximum efficiency $\eta_C^{\text{hybrid}}$ which can again exceed the effective Carnot efficiency $\eta_C^e$. The EMP and the maximum power can be also derived.

## V. CONCLUSION

We demonstrated that the power and the efficiency of a device working in nonequilibrium active environments with Gaussian colored noises with finite persistent time can overcome the conventional Carnot limit. This is possible because the total EP in the steady state cannot be expressed solely by the Clausius EP, and the unconventional EP term [28,29] emerges from the non-Marcovianity of the active reservoirs [25] (equivalently, a velocity-dependent force present in the underdamped representation). In fact, the Clausius EP is negative for overcoming the Carnot bound, which is compensated by the positive contribution from the unconventional EP. This gives rise to the nonnegative total EP, which is fully consistent with the thermodynamic second law. Thus, this unconventional EP can be regarded as the mathematical expression for the additional cost to maintain the steady state of active reservoirs.

We emphasize that our main results can be also applied to more general cases with non-Gaussian colored noises and an arbitrary nonlinear potential. This implies that the non-Markovianity of the active noise is more crucial than its non-Gaussianity for the out-performance of the active engine, in contrast to the recent claim by Krishnamurthy *et al.* [10]. Furthermore, we find that the timescale symmetry breaking between two active reservoirs is necessary for the supremacy of the active engine.

Our result is readily realizable and applicable to the energy harvesting devices in bacterial or active baths. Thus, our conclusion provides a new way of developing high-performance energy-harvesting devices harnessing energy of microorganisms which exist almost everywhere in nature.

## ACKNOWLEDGMENTS

Authors acknowlege the Korea Institute for Advanced Study for providing computing resources (KIAS Center for Advanced Computation Linux Cluster System). This research was supported by NRF Grant No. 2017R1D1A1B06035497 (H.P.) and KIAS individual Grants No. PG013604 (H.P.), No. PG074001 (J.M.P.), and No. QP064902 (J.S.L.) at Korea Institute for Advanced Study.

## APPENDIX A: COVARIANT MATRIX, STEADY-STATE DISTRIBUTION, WORK, AND HEAT RATES IN THE ORNSTEIN-UHLENBECK PROCESS

The multivariate Ornstein-Uhlenbeck process [33,37] is described by

$$d\mathbf{z} = -\mathsf{A}\mathbf{z}dt + d\Xi, \tag{A1}$$

where $\mathbf{z}$ is a $d$-dimensional state (column) vector and $\mathsf{A}$ is a linear force matrix. The noise vector $d\Xi$ satisfies $\langle d\Xi(t)\rangle = 0$ and $\langle d\Xi(t)d\Xi^{\mathsf{T}}(t)\rangle = 2\mathsf{D}dt$, where $\mathsf{D}$ is a symmetric diffusion matrix. Note that the superscript "$\mathsf{T}$" represents the transpose.

The covariant matrix $\Sigma$ is defined as

$$\Sigma = \langle \mathbf{z}\mathbf{z}^{\mathsf{T}}\rangle_s = \Sigma^{\mathsf{T}}, \tag{A2}$$

where $\langle\cdots\rangle_s$ denotes the steady-state average. Its incremental satisfies

$$\begin{aligned} d\Sigma &= \langle d\mathbf{z}\circ\mathbf{z}^{\mathsf{T}}\rangle_s + \langle \mathbf{z}\circ d\mathbf{z}^{\mathsf{T}}\rangle_s \\ &= [-\mathsf{A}\Sigma - \Sigma\mathsf{A}^{\mathsf{T}} + 2\mathsf{D}]dt = 0, \end{aligned} \tag{A3}$$

with the Stratonovich multiplication $\circ$, and thus we obtain

$$\mathsf{A}\Sigma + \Sigma\mathsf{A}^{\mathsf{T}} = 2\mathsf{D}. \tag{A4}$$

Similarly, we find

$$\langle \mathbf{z}\circ\dot{\mathbf{z}}^{\mathsf{T}}\rangle_s = -\Sigma\mathsf{A}^{\mathsf{T}} + \mathsf{D}, \tag{A5}$$

which is useful for calculation of work and heat rates.

The steady-state distribution is given as [33,37]

$$P(\mathbf{z}) = \frac{1}{\sqrt{|2\pi\,\Sigma|}}\exp\left[-\frac{1}{2}\mathbf{z}^{\mathsf{T}}\Sigma^{-1}\mathbf{z}\right], \tag{A6}$$

where $|\cdots|$ is the determinant. The stability condition for the steady state is obtained by requiring the positivity of all eigenvalues of the covaraint matrix $\Sigma$ or, equivalently, of the linear force matrix $\mathsf{A}$ for the nonnegative diagonal diffusion matrix $\mathsf{D}$.

### 1. Equilibrium-reservoir engine

The equations of motion are given in Eqs. (1) and (2). Then the state vector is defined as $\mathbf{z} = (x_1, x_2)^{\mathsf{T}}$ with

$$\mathsf{A} = \begin{pmatrix} \frac{k}{\gamma_1} & -\frac{\epsilon}{\gamma_1} \\ -\frac{\delta}{\gamma_2} & \frac{k}{\gamma_2} \end{pmatrix}, \quad \mathsf{D} = \begin{pmatrix} \frac{T_1}{\gamma_1} & 0 \\ 0 & \frac{T_2}{\gamma_2} \end{pmatrix}. \tag{A7}$$

Solving Eq. (A4), we find

$$\begin{aligned} \Sigma_{11} &= \langle x_1^2 \rangle_s = \frac{T_1[k^2\gamma_1 + (k^2 - K)\gamma_2] + T_2\epsilon^2\gamma_2}{k(\gamma_1+\gamma_2)(k^2-K)}, \\ \Sigma_{12} &= \langle x_1 x_2 \rangle_s = \frac{T_1\delta\gamma_1 + T_2\epsilon\gamma_2}{(\gamma_1+\gamma_2)(k^2-K)}, \\ \Sigma_{22} &= \langle x_2^2 \rangle_s = \frac{T_1\delta^2\gamma_1 + T_2[k^2\gamma_2 + (k^2-K)\gamma_1]}{k(\gamma_1+\gamma_2)(k^2-K)}, \end{aligned} \tag{A8}$$

with $K = \delta\epsilon$. Note that $\Sigma$ is invariant under the time rescaling as $\gamma_i \to a\gamma_i$ with fixed $T_i$. With these results, we get from Eq. (A5)

$$\begin{aligned} \langle x_1 \dot{x}_2 \rangle_s &= (-\Sigma\mathsf{A}^{\mathsf{T}} + \mathsf{D})_{12} \\ &= -\Sigma_{11}\mathsf{A}_{21} - \Sigma_{12}\mathsf{A}_{22} = \frac{T_1\delta - T_2\epsilon}{k(\gamma_1+\gamma_2)}. \end{aligned} \tag{A9}$$

For stability, we diagonalize $\mathsf{A}$ with two eigenvalues as

$$\lambda^{\pm} = \frac{k(\gamma_1+\gamma_2) \pm \sqrt{k^2(\gamma_1+\gamma_2)^2 + 4\gamma_1\gamma_2(K-k^2)}}{2\gamma_1\gamma_2}. \tag{A10}$$

For a stable solution, the real part of all eigenvalues of $\mathsf{A}$ should be positive. Thus, the stability condition is given by

$$K < k^2. \tag{A11}$$

### 2. Effective temperature of a single active or hybrid reservoir

We consider a one-dimensional overdamped linear system in contact with a single hybrid reservoir as

$$\gamma\dot{x} = -kx + \zeta + \sqrt{2\gamma T}\xi', \quad \tau\dot{\zeta} = -\zeta + \sqrt{2D}\xi, \tag{A12}$$

with $\langle \xi'(t)\xi'(t') \rangle = \delta(t-t')$ and $\langle \xi(t)\xi(t') \rangle = \delta(t-t')$. One can recover the active-reservoir case by setting $T = 0$. With the state vector $\mathbf{z} = (x, \zeta)^{\mathsf{T}}$, we have

$$\mathsf{A} = \begin{pmatrix} \frac{k}{\gamma} & -\frac{1}{\gamma} \\ 0 & \frac{1}{\tau} \end{pmatrix}, \quad \mathsf{D} = \begin{pmatrix} \frac{T}{\gamma} & 0 \\ 0 & \frac{D}{\tau^2} \end{pmatrix}. \tag{A13}$$

Then, Eq. (A4) yields

$$\begin{aligned} &\Sigma_{11} = \langle x^2 \rangle_s = \frac{1}{k}\left(T + \frac{D}{\Gamma}\right), \quad \Sigma_{12} = \langle x\zeta \rangle_s = \frac{D}{\Gamma}, \\ &\Sigma_{22} = \langle \zeta^2 \rangle_s = \frac{D}{\tau} \quad \text{with} \quad \Gamma = \gamma + k\tau. \end{aligned} \tag{A14}$$

Inverting $\Sigma$, we get the steady state given by Eq. (A6) in terms of $\mathbf{z}$. The steady state of the true dynamic variable $x$ can be obtained by integrating Eq. (A6) over $\zeta$ as

$$P(x) = \frac{1}{\sqrt{2\pi\,\Sigma_{11}}} \exp\left[-\frac{x^2}{2\Sigma_{11}}\right] = \sqrt{\frac{k}{2\pi T^e}} \exp\left[-\frac{kx^2}{2T^e}\right], \tag{A15}$$

with the effective temperature $T^e = T + D/\Gamma$. For the active engine without a nonconservative force (no coupling between two engine degrees of freedom, $x_1$ and $x_2$), we get Eq. (11) for the stationary distribution with $T = 0$.

### 3. Active-reservoir engine

The equations of motion for the active-reservoir engine are given in Eqs. (9) and (10).

The state vector is defined as $\mathbf{z} = (x_1, x_2, \zeta_1, \zeta_2)^{\mathsf{T}}$ with

$$\mathsf{A} = \begin{pmatrix} \frac{k}{\gamma_1} & -\frac{\epsilon}{\gamma_1} & -\frac{1}{\gamma_1} & 0 \\ -\frac{\delta}{\gamma_2} & \frac{k}{\gamma_2} & 0 & -\frac{1}{\gamma_2} \\ 0 & 0 & \frac{1}{\tau_1} & 0 \\ 0 & 0 & 0 & \frac{1}{\tau_2} \end{pmatrix},$$

$$\mathsf{D} = \begin{pmatrix} 0 & 0 & 0 & 0 \\ 0 & 0 & 0 & 0 \\ 0 & 0 & \frac{D_1}{\tau_1^2} & 0 \\ 0 & 0 & 0 & \frac{D_2}{\tau_2^2} \end{pmatrix}. \tag{A16}$$

Solving Eq. (A4), we find

$$\begin{aligned} \Sigma_{11} &= \frac{1}{k(\gamma_1+\gamma_2)(k^2-K)}\left[\frac{D_1\{k^2(\gamma_2\Gamma_1 + k\gamma_1\tau_1) + (k^2-K)\gamma_2^2\}}{\gamma_2\Gamma_1\mathcal{A}_K} + \frac{\epsilon^2 D_2(\gamma_1\Gamma_2 + k\gamma_2\tau_2)}{\gamma_1\Gamma_2\mathcal{B}_K}\right], \\ \Sigma_{12} &= \frac{1}{(\gamma_1+\gamma_2)(k^2-K)}\left[\frac{\delta D_1(\gamma_2\Gamma_1 + k\gamma_1\tau_1)}{\gamma_2\Gamma_1\mathcal{A}_K} + \frac{\epsilon D_2(\gamma_1\Gamma_2 + k\gamma_2\tau_2)}{\gamma_1\Gamma_2\mathcal{B}_K}\right], \\ \Sigma_{22} &= \frac{1}{k(\gamma_1+\gamma_2)(k^2-K)}\left[\frac{\delta^2 D_1(\gamma_2\Gamma_1 + k\gamma_1\tau_1)}{\gamma_2\Gamma_1\mathcal{A}_K} + \frac{D_2\{k^2(\gamma_1\Gamma_2 + k\gamma_2\tau_2) + (k^2-K)\gamma_1^2\}}{\gamma_1\Gamma_2\mathcal{B}_K}\right], \\ \Sigma_{13} &= \frac{D_1(\gamma_2 + k\tau_1)}{\gamma_2\Gamma_1\mathcal{A}_K}, \quad \Sigma_{14} = \frac{\epsilon D_2\tau_2}{\gamma_1\Gamma_2\mathcal{B}_K}, \quad \Sigma_{23} = \frac{\delta D_1\tau_1}{\gamma_2\Gamma_1\mathcal{A}_K}, \quad \Sigma_{24} = \frac{D_2(\gamma_1 + k\tau_2)}{\gamma_1\Gamma_2\mathcal{B}_K}, \\ \Sigma_{33} &= \frac{D_1}{\tau_1}, \quad \Sigma_{34} = 0, \quad \Sigma_{44} = \frac{D_2}{\tau_2}, \end{aligned} \tag{A17}$$

where $\mathcal{A}_K$ and $\mathcal{B}_K$ are given in Eq. (13) with $K = \delta\epsilon$ and $\Gamma_i = \gamma_i + k\tau_i$. As expected, $\Sigma$ is invariant under the time rescaling as $\gamma_i \to a\gamma_i$, $D_i \to aD_i$, and $\tau_i \to a\tau_i$,.

From Eq. (A5), we get

$$\begin{aligned}\langle x_1\dot{x}_2\rangle_s &= (-\Sigma\mathsf{A}^{\mathsf{T}} + \mathsf{D})_{12} = -\Sigma_{11}\mathsf{A}_{21} - \Sigma_{12}\mathsf{A}_{22} - \Sigma_{14}\mathsf{A}_{24}, \\ &= \frac{1}{k(\gamma_1+\gamma_2)}\left[\frac{D_1\delta}{\Gamma_1\mathcal{A}_K} - \frac{D_2\epsilon}{\Gamma_2\mathcal{B}_K}\right] \\ &= \frac{1}{k(\gamma_1+\gamma_2)}\left[\frac{T_1^e\delta}{\mathcal{A}_K} - \frac{T_2^e\epsilon}{\mathcal{B}_K}\right], \end{aligned} \tag{A18}$$

with the effective temperatures $T_i^e = D_i/\Gamma_i$. The stability condition is the same as before in Eq. (A11), which can be clearly seen from the force matrix $\mathsf{A}$ in Eq. (A16).

There are some interesting cases considered. First, in the case of the equilibrium reservoirs ($\tau_1 = \tau_2 = 0$), we have $\mathcal{A}_K = \mathcal{B}_K = 1$ and $T_i^e = T_i = D_i/\gamma_i$, and then the conventional result, Eq. (5), is recovered. For $T_1 = T_2$, $\langle\dot{W}\rangle_s = (\epsilon - \delta)\langle x_1\dot{x}_2\rangle_s = -(\delta-\epsilon)^2 T_1/[k(\gamma_1+\gamma_2)] \leqslant 0$, which implies that no positive work extraction is possible with the same-temperature equilibrium reservoirs. Note that the timescale does not enter here, i.e., we get the same result with $\gamma_1 = a\gamma_2$ and $D_1 = aD_2$ for general positive $a$.

Second, we consider the case with the same effective temperatures ($T_1^e = T_2^e$) with different timescales such that $\tau_1 = a\tau_2$, $\gamma_1 = a\gamma_2$, and $D_1 = aD_2$. As $\mathcal{A}_K \neq \mathcal{B}_K$ except for $a = 1$, the positive work extraction is possible ($\langle\dot{W}\rangle_s > 0$) for $a < 1$ where $\mathcal{B}_K > \mathcal{A}_K$. This implies that the active reservoir with a shorter timescale is effectively hotter than the active reservoir with a longer one. Thus, in order to understand the thermodynamics, the active reservoir must be characterized not only by the effective temperature but also by the timescale. At $a = 1$, two active reservoirs become identical (or considered as a single active reservoir) and the work production is nonpositive; $\langle\dot{W}\rangle_s \sim -(\delta-\epsilon)^2 \leqslant 0$. The $a > 1$ case will be discussed later.

Third, we consider the case with the same timescale ($\gamma_1 = \gamma_2$ and $\tau_1 = \tau_2$) with different noise strengths ($D_1 > D_2$). So the effective temperatures $T_1^e > T_2^e$. The *timescale symmetry* between two active reservoirs implies not only the same persistence time but also the same physical property of the reservoir-system contact for two active reservoirs. In this case, $\Gamma_1 = \Gamma_2$, $\mathcal{A}_K = \mathcal{B}_K$, and all energetic quantities are essentially the same as those in the equilibrium-reservoir case with the effective temperatures except for the overall factor $1/\mathcal{A}_K$. Thus, the efficiency is bounded by the (effective) Carnot efficiency, $\eta \leqslant \eta_C^e = 1 - T_2^e/T_1^e = 1 - T_2/T_1 = \eta_C$. In order to surpass the Carnot efficiency, this symmetry should be broken. In a very recent paper [11] studying a stochastic Stirling engine with active baths, only the timescale symmetric case was considered and no better efficiency was found with these simple active reservoirs. If the symmetry is broken in this Stirling engine model, then we can show that the efficiency for the active reservoirs can surpass that for the equilibrium reservoirs. The importance of the symmetry was also pointed out recently in some quantum heat engines in order to enhance the engine performance [41,42].

Finally, it is remarkable to see that the heat flow can be reversed when $T_2^e/\mathcal{B}_K > T_1^e/\mathcal{A}_K$ with $T_1^e \geqslant T_2^e$ (including the $a > 1$ case in the above) and the work extraction is still positive. In the equilibrium-reservoir case, one can devise a refrigerator instead of a heat engine ($\langle\dot{Q}_1\rangle_s < 0$ and $\langle\dot{Q}_2\rangle_s > 0$), but the thermodynamic second law with the Clausius entropy production demands the work input ($\langle\dot{W}\rangle_s < 0$). Thus, one should do work on the system in order to extract heat from the low-temperature reservoir. However, in the active-reservoir engine, it is possible to make the heat flow from the low effective-temperature reservoir ($\langle\dot{Q}_2\rangle_s > 0$) and do work outside ($\langle\dot{W}\rangle_s > 0$) and the remaining heat dissipates into the high-effective-temperature reservoir ($\langle\dot{Q}_1\rangle_s < 0$.) See Fig. 2. In this case, one should define the efficiency as $\eta = \langle\dot{W}\rangle_s/\langle\dot{Q}_2\rangle_s = 1 - \epsilon/\delta$. We note that this is fully consistent with the thermodynamic second law due to the presence of an *unconventional* EP term [28,29], which will be discussed later in Appendix C.

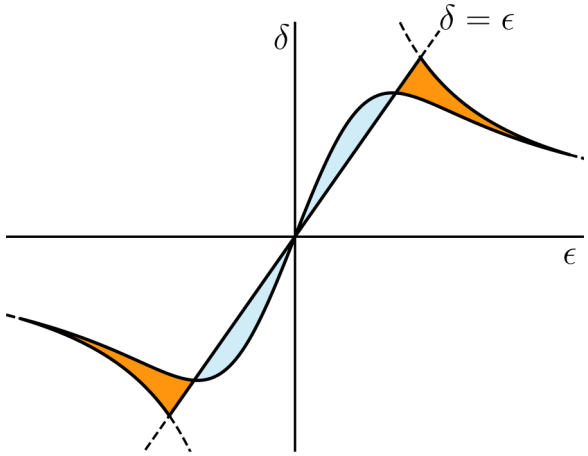


FIG. 2. Engine with active reservoirs with the reverse heat flows. Shaded areas, enclosed by the curves $\delta = \epsilon$, $\epsilon\delta = k^2$, and $T_1^e\delta/\mathcal{A}_K = T_2^e\epsilon/\mathcal{B}_K$, denote the areas in which the device works as a stable and useful engine with positive work extraction. The orange region denotes the normal-engine area, while the sky blue region denotes the engine area with the reversed heat flows. For this plot, $\tau_1 = 16$, $\gamma_1 = 0.1$, $D_1 = 7$, and $k = \tau_2 = \gamma_2 = D_2 = 1$ are used.

#### 4. Hybrid-reservoir engine

The equations of motion for the hybrid-reservoir engine are given in Eqs. (2) and (17).

The state vector is defined as $\mathbf{z} = (x_1, x_2, \zeta_1, \zeta_2)^{\mathsf{T}}$ with

$$\mathsf{A} = \begin{pmatrix} \frac{k}{\gamma_1} & -\frac{\epsilon}{\gamma_1} & -\frac{1}{\gamma_1} & 0 \\ -\frac{\delta}{\gamma_2} & \frac{k}{\gamma_2} & 0 & -\frac{1}{\gamma_2} \\ 0 & 0 & \frac{1}{\tau_1} & 0 \\ 0 & 0 & 0 & \frac{1}{\tau_2} \end{pmatrix},$$

$$\mathsf{D} = \begin{pmatrix} \frac{T_1}{\gamma_1} & 0 & 0 & 0 \\ 0 & \frac{T_2}{\gamma_2} & 0 & 0 \\ 0 & 0 & \frac{D_1}{\tau_1^2} & 0 \\ 0 & 0 & 0 & \frac{D_2}{\tau_2^2} \end{pmatrix}. \tag{A19}$$

Solving Eq. (A4), we find that the covariant matrix is given by the simple sum of the covariant matrices for the equilibrium reservoirs in Eq. (A8) and for the active reservoirs in Eq. (A17). The matrix elements for $\Sigma_{13}$, $\Sigma_{14}$, $\Sigma_{23}$, $\Sigma_{24}$, $\Sigma_{33}$, $\Sigma_{34}$, and $\Sigma_{44}$ are identical to those for the active reservoirs in Eq. (A17). From Eq.(A5), we easily get

$$\langle x_1 \dot{x}_2 \rangle_s = (-\Sigma \mathsf{A}^{\mathsf{T}} + \mathsf{D})_{12} = -\Sigma_{11}\mathsf{A}_{21} - \Sigma_{12}\mathsf{A}_{22} - \Sigma_{14}\mathsf{A}_{24}, = \frac{1}{k(\gamma_1+\gamma_2)}\left[T_1\delta - T_2\epsilon + \frac{D_1\delta}{\Gamma_1\mathcal{A}_K} - \frac{D_2\epsilon}{\Gamma_2\mathcal{B}_K}\right], \tag{A20}$$

which is also the simple sum of Eqs. (A9) and (A18). The stability condition is the same as before in Eq. (A11), which can be clearly seen from the force matrix $\mathsf{A}$ in Eq. (A19).

## APPENDIX B: POWER AND EFFICIENCY FOR AN ACTIVE-RESERVOIR ENGINE

The activeness of a reservoir $i$ is characterized by the persistent time $\tau_i$. A nonzero $\tau_i$ lowers the reservoir temperature effectively as $T_i^e = T_i/[1 + k\tau_i/\gamma_i] < T_i$ by itself and increases the value of the factor $\mathcal{A}_K$ ($\mathcal{B}_K$) when it is combined with another reservoir [see Eq. (13)]. Note that both of $\mathcal{A}_K$ and $\mathcal{B}_K$ monotonically increase with $\tau_1$ and $\tau_2$, respectively.

The power and efficiency of an active engine depend on the activeness of both hot and cold reservoirs. The maximum efficiency $\eta_C^a$ is also a function of $\tau_1$ and $\tau_2$ as seen in Eq. (14). Figure 3(a) shows the $\tau_2$-dependent behavior of $\eta_C^a$ for various values of $\tau_1 = 0, 0.2, 0.4$, and $0.6$ with parameters $k = 2$, $\gamma_1 = 1$, $\gamma_2 = 1$, $T_1^e = 2$, $T_2^e = 1$, and $K = 2$. As the figure shows, $\eta_C^a$ is a monotonically increasing function of $\tau_2$ and gets lowered as $\tau_1$ increases. With $\tau_1 = 0$ (discussed in the main text), $\eta_C^a$ is always larger than $\eta_C^e$, whereas it becomes smaller than $\eta_C^e$ for small $\tau_2$ when $\tau_1 > 0$. We note that a similar dependence of $\eta_C^a$ on $\tau_1$ and $\tau_2$ arises when $T_i = D_i/\gamma_i$ is fixed instead of fixed $T_i^e$. In the case when the heat flow is reversed, discussed in Appendix A3, the efficiency should be redefined which is not shown here.

The local maximum power is obtained at the optimal value $\delta_m = \sqrt{T_2^e\mathcal{A}_K/(T_1^e\mathcal{B}_K)}\epsilon_m$ for fixed $K$. At the optimal value, the local maximum power and the efficiency at the local maximum power are given by

$$\langle \dot{W} \rangle_s^m = \frac{K}{k(\gamma_1+\gamma_2)}\left(\sqrt{\frac{T_1^e}{\mathcal{A}_K}} - \sqrt{\frac{T_2^e}{\mathcal{B}_K}}\right)^2 \quad \text{and}$$

$$\eta_m = 1 - \sqrt{\frac{T_2^e\mathcal{A}_K}{T_1^e\mathcal{B}_K}}, \tag{B1}$$

respectively. Their behaviors are similar to those of $\eta_C^a$ as shown in Figs. 3(b) and 3(c).

## APPENDIX C: ENTROPY PRODUCTION RATE FOR AN ACTIVE-RESERVOIR ENGINE

We consider an underdamped dynamics with a velocity-dependent force with multiple equilibrium reservoirs such as

$$d\mathbf{x} = \mathbf{v}dt, \quad \mathsf{M}d\mathbf{v} = \mathbf{f}(\mathbf{x},\mathbf{v})dt - \mathsf{G}\mathbf{v}dt + d\Xi, \tag{C1}$$

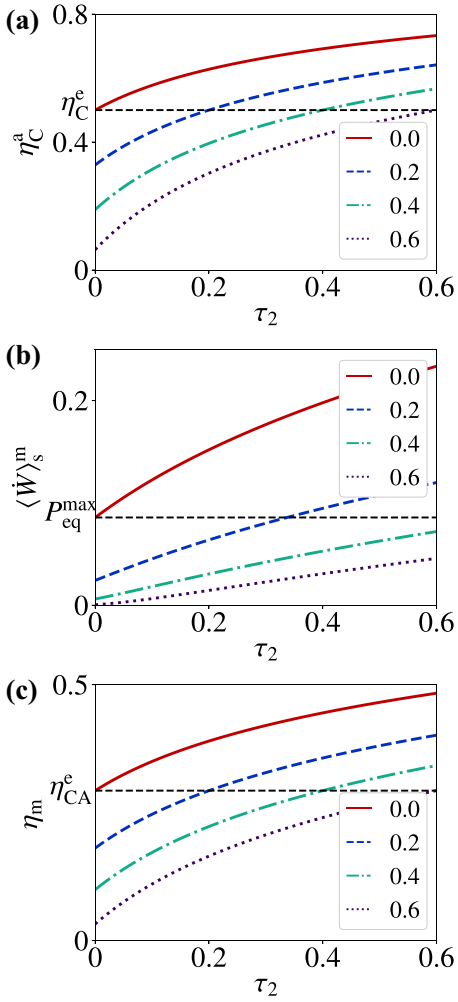


FIG. 3. $\tau_2$-dependent behavior of (a) the maximum efficiency $\eta_C^a$, (b) the local maximum power $\langle \dot{W} \rangle_s^m$, and (c) the efficiency at the maximum power $\eta_m$, for $\tau_1 = 0$ (red solid curve), 0.2 (blue dashed curve), 0.4 (cyan dash-dotted curve), and 0.6 (magenta dotted curve). Black dashed lines indicate the conventional limit of a passive engine with the effective temperatures.

where $\mathsf{M}$ is a mass matrix, $\mathsf{G}$ is a friction matrix, and the noise satisfies $\langle d\Xi(t)\rangle = 0$ and $\langle d\Xi(t) d\Xi^{\mathsf{T}}(t)\rangle = 2\mathsf{D}dt$ with $\mathsf{D} = \mathsf{D}^{\mathsf{T}}$. The force $\mathbf{f}$ can be divided into the reversible and irreversible parts, $\mathbf{f} = \mathbf{f}^r + \mathbf{f}^{\rm ir}$, such that $\mathbf{f}^r(\mathbf{z}) = \mathbf{f}^r(\varepsilon\mathbf{z})$ and $\mathbf{f}^{\rm ir}(\mathbf{z}) = -\mathbf{f}^{\rm ir}(\varepsilon\mathbf{z})$, with the state vector $\mathbf{z} = (\mathbf{x}, \mathbf{v})$ and the parity operator $\varepsilon$ defined by $\varepsilon\mathbf{z} = (\mathbf{x}, -\mathbf{v})$ [28,37].

The environmental EP during an infinitesimal time increment is given by

$$dS_{\rm env} = \ln\frac{\Pi(\mathbf{z}', t+dt|\mathbf{z}, t)}{\Pi(\varepsilon\mathbf{z}, t+dt|\varepsilon\mathbf{z}', t)}, \tag{C2}$$

where $\Pi$ is the conditional probability for a given trajectory [28,44]. Then straightforward algebra yields

$$dS_{\rm env} = -(\mathsf{M}d\mathbf{v} - \mathbf{f}^r dt)^{\mathsf{T}}\mathsf{D}^{-1} \circ (\mathsf{G}\mathbf{v} - \mathbf{f}^{\rm ir}) - \partial_{\mathbf{v}}\mathsf{M}^{-1}\mathbf{f}^r dt. \tag{C3}$$

A similar expression is shown in Eq. (11) in Ref. [28] for the mass matrix $\mathsf{M} = m\mathsf{I}$ with the identity matrix $\mathsf{I}$.

Then the standard stochastic calculus gives the average environmental EP rate as

$$\langle \dot{S}_{\rm env}\rangle = \langle (\mathbf{f}^{\rm ir} - \mathsf{G}\mathbf{v})^{\mathsf{T}}\mathsf{D}^{-1}(\mathbf{f}^{\rm ir} - \mathsf{G}\mathbf{v})\rangle - {\rm Tr}(\mathsf{G}\mathsf{M}^{-1}) - \langle \partial_{\mathbf{v}}\mathsf{M}^{-1}(\mathbf{f}^{r} - \mathbf{f}^{\rm ir})\rangle, \tag{C4}$$

which is usually divided into the conventional Clausius EP term and the so-called *unconventional* extra EP term, see Eqs. (25) and (26) in Ref. [28,29]. However, in the active-reservoir problem, the heat current flowing from the active reservoir contains the work done by the velocity-dependent force in the underdamped representation [see Eq. (16)]. Thus, it is not useful to divide the EP term in that way.

Now we restrict ourselves to a simple linear force such as

$$\mathbf{f}(\mathbf{x},\mathbf{v}) = -\mathsf{K}\mathbf{x} + \mathsf{B}\mathbf{v}, \tag{C5}$$

which corresponds to our case in Eq. (16) with $\mathbf{f}^{r} = -\mathsf{K}\mathbf{x}$ and $\mathbf{f}^{\rm ir} = \mathsf{B}\mathbf{v}$. In this case, it is convenient to rewrite the equations of motion as

$$d\mathbf{x} = \mathbf{v}dt, \quad \mathsf{M}d\mathbf{v} = -\mathsf{K}\mathbf{x}dt - \tilde{\mathsf{G}}\mathbf{v}dt + d\Xi, \tag{C6}$$

with the new friction matrix $\tilde{\mathsf{G}} = \mathsf{G} - \mathsf{B}$, which is not diagonal with off-diagonal elements in $\mathsf{B}$ for the Lorentz-like force. As the irreversible part of the force is absorbed into the friction matrix, we have the reversible force only. Then, Eq. (C4) reads

$$\begin{aligned}\langle \dot{S}_{\rm env}\rangle &= \langle (\tilde{\mathsf{G}}\mathbf{v})^{\mathsf{T}}\mathsf{D}^{-1}(\tilde{\mathsf{G}}\mathbf{v})\rangle - {\rm Tr}(\tilde{\mathsf{G}}\mathsf{M}^{-1}),\\ &= {\rm Tr}(\tilde{\mathsf{G}}^{\mathsf{T}}\mathsf{D}^{-1}\tilde{\mathsf{G}}\Sigma^{\mathbf{v}}) - {\rm Tr}(\tilde{\mathsf{G}}\mathsf{M}^{-1}),\end{aligned} \tag{C7}$$

where the velocity-velocity correlation matrix $\Sigma^{\mathbf{v}} = \langle \mathbf{v}\mathbf{v}^{\mathsf{T}}\rangle$.

It is interesting to introduce the *active* heat matrix differential as

$$d\mathsf{Q}^{a} \equiv [-\tilde{\mathsf{G}}\mathbf{v}dt + d\Xi]\circ\mathbf{v}^{\mathsf{T}}. \tag{C8}$$

The diagonal part of the heat matrix corresponds to the heat flow from each active reservoir, discussed in the paragraph below Eq. (16); $\mathsf{Q}^{a}_{ii} = Q^{a}_{i}$. A simple stochastic calculus yields

$$\langle \dot{\mathsf{Q}}^{a}\rangle^{\mathsf{T}} = -\langle \mathbf{v}(\tilde{\mathsf{G}}\mathbf{v})^{\mathsf{T}}\rangle + \mathsf{M}^{-1}\mathsf{D}. \tag{C9}$$

In order to relate the heat matrix to the environmental EP, we also introduce the *effective* temperature matrix as

$$\mathcal{T}^{e} \equiv \tilde{\mathsf{G}}^{-1}\mathsf{D}. \tag{C10}$$

Then, one can easily find

$$\langle \dot{S}_{\rm env}\rangle = -{\rm Tr}[(\mathcal{T}^{e})^{-1}\langle \dot{\mathsf{Q}}^{a}\rangle^{\mathsf{T}}], \tag{C11}$$

which is similar to the *generalized* Clausius relation discussed in Ref. [28].

We now focus on our specific problem given in Eq. (16) with

$$\mathsf{M} = \begin{pmatrix} m_1 & 0\\ 0 & m_2\end{pmatrix}, \quad \mathsf{K} = \begin{pmatrix} k & -\epsilon\\ -\delta & k\end{pmatrix}, \quad \mathsf{B} = \begin{pmatrix} 0 & \epsilon\tau_1\\ \delta\tau_2 & 0\end{pmatrix},$$
$$\mathsf{D} = \begin{pmatrix} D_1 & 0\\ 0 & D_2\end{pmatrix}, \quad \tilde{\mathsf{G}} = \begin{pmatrix} \Gamma_1 & -\epsilon\tau_1\\ -\delta\tau_2 & \Gamma_2\end{pmatrix}, \tag{C12}$$

where $m_i = \gamma_i\tau_i$. In the steady state, the environment EP is equivalent to the total EP, $\langle \dot{S}\rangle_s$, and $\Sigma^{\mathbf{v}}$ can be easily calculated from the steady-state covariant matrix for the active-reservoir engine in Eq. (A17), using the identities as

$$\Sigma^{\mathbf{v}}_{ij} = \langle \mathbf{v}_i\mathbf{v}_j\rangle_s = \langle \dot{\mathbf{x}}_i\dot{\mathbf{x}}_j\rangle_s = \left\langle (\mathsf{A}\mathbf{z})_i(\mathsf{A}\mathbf{z})^{\mathsf{T}}_j\right\rangle_s = (\mathsf{A}\Sigma\mathsf{A}^{\mathsf{T}})_{ij}, \tag{C13}$$

where $i,j = 1,2$ and $\mathsf{A}$ and $\Sigma$ are the linear force matrix and the covariant matrix in Eq. (A17), respectively.

After a lengthy but straightforward algebra for Eq. (C7), we finally obtain the total EP in the steady state of the active-reservoir engine as

$$\langle \dot{S}\rangle_s = -\frac{\langle \dot{Q}_1\rangle_s\mathcal{A}_K}{T^{e}_1} - \frac{\langle \dot{Q}_2\rangle_s\mathcal{B}_K}{T^{e}_2} + (\tau_1 - \tau_2)\left[\frac{\tau_1\epsilon^2}{\tau_2\gamma_2\Gamma_1\mathcal{B}_K}\left(\frac{T^{e}_2}{T^{e}_1}\right) - \frac{\tau_2\delta^2}{\tau_1\gamma_1\Gamma_2\mathcal{A}_K}\left(\frac{T^{e}_1}{T^{e}_2}\right)\right], \tag{C14}$$

with $\langle \dot{Q}_i\rangle_s = \langle \dot{Q}^{a}_i\rangle_s = \langle \dot{\mathsf{Q}}^{a}_{ii}\rangle_s$, which is given by Eq. (A18). As usual, the thermodynamic second law guarantees the nonnegativity of the total EP, i.e., $\langle \dot{S}\rangle_s \geqslant 0$. Note that the first two terms look like Clausius EP terms with the *modified* effective temperatures $T^{e}_1/\mathcal{A}_K$ and $T^{e}_2/\mathcal{B}_K$, but the third term seems not related to any simple physical observable. The unconventional EP term appearing generally in the underdamped dynamics with velocity-dependent forces [28] contributes to both the modified Clausius EP term and the extra third term. Interestingly, the modified Clausius EP term turns out to be always nonnegative in this specific problem, i.e.,

$$\langle \dot{S}_{\rm mClau}\rangle_s = -\frac{\langle \dot{Q}_1\rangle_s\mathcal{A}_K}{T^{e}_1} - \frac{\langle \dot{Q}_2\rangle_s\mathcal{B}_K}{T^{e}_2} = \frac{\mathcal{A}_K\mathcal{B}_K}{k(\gamma_1+\gamma_2)T^{e}_1T^{e}_2}\left[\frac{T^{e}_1\delta}{\mathcal{A}_K} - \frac{T^{e}_2\epsilon}{\mathcal{B}_K}\right]^2 \geqslant 0. \tag{C15}$$

Along the maximum efficiency line ($\eta = \eta^{a}_{C}$) in Fig. 1(d) derived from Eq. (12), this modified Clausius EP rate vanishes just like in the equilibrium-reservoir case where the maximum efficiency is obtained in the reversible process (zero EP rate). However, the true EP along the maximum efficiency line does not vanish due to the extra EP term in Eq. (C14).

As the value of the extra EP term can be positive, negative, or zero depending on the parameter values, there is no inequality between the true EP and the modified Clausius EP, in general. Nevertheless, when the persistence time is the same for both active reservoirs ($\tau_1 = \tau_2$), the modified Clausius EP becomes exactly identical to the total EP. Therefore, in this special case, all physical quantities including the heat, work, EP for the active-reservoir engine dynamics turn out be equivalent to those for the equilibrium-reservoir engine with the modified effective temperatures, $T^{e}_1/\mathcal{A}_K$ and $T^{e}_2/\mathcal{B}_K$. For a more special case with the symmetric timescale ($\tau_1 = \tau_2$ and $\gamma_1 = \gamma_2$) discussed before, the (modified effective) temperature ratio is identical to the equilibrium temperature ratio and all physical quantities become identical to those for the equilibrium-reservoir engine with the temperatures $T_1$ and $T_2$ except for the overall timescale factor.

[1] R. J. M. Vullers, R. van Schaijk, I. Doms, C. Van Hoof, and R. Mertens, Micropower energy harvesting, Solid-State Electron. **53**, 684 (2009).

[2] L. Mateu and F. Moll, Review of energy harvesting techniques and applications for microelectronics, Proc. SPIE **5837**, 359 (2005).

[3] P. M. Thibado, P. Kumar, S. Singh, M. Ruiz-Garcia, A. Lasanta, and L. L. Bonilla, Fluctuation-induced current from freestanding graphene: Toward nanoscale energy harvesting, arXiv:2002.09947.

[4] M. Josefsson, A. Svilans, A. M. Burke, E. A. Hoffmann, S. Fahlvik, C. Thelander, M. Leijnse, and H. Linke, A quantum-dot heat engine operating close to the thermodynamic efficiency limits, Nat. Nanotech. **13**, 920 (2018).

[5] N. Femia, G. Petrone, G. Spagnuolo, and M. Vitelli, *Power Electronics and Control Techniques for Maximum Energy Harvesting in Photovoltaic Systems*, 1st ed. (CRC Press, Boca Raton, FL, 2013).

[6] H. S. Kim, J.-H. Kim, and J. Kim, A review of piezoelectric energy harvesting based on vibration, Int. J. Precis. Eng. Man. **12**, 1129 (2011).

[7] W. Niedenzu, V. Mukherjee, A. Ghosh, A. G. Kofman, and G. Kurizki, Quantum engine efficiency bound beyond the second law of thermodynamics, Nat. Commun. **9**, 165 (2018).

[8] J. Klaers, S. Faelt, A. Imamoglu, and E. Togan, Squeezed Thermal Reservoirs as a Resource for a Nanomechanical Engine Beyond the Carnot Limit, Phys. Rev. X **7**, 031044 (2017).

[9] J. Roßnagel, O. Abah, F. Schmidt-Kaler, K. Singer, and E. Lutz, Nanoscale Heat Engine Beyond the Carnot Limit, Phys. Rev. Lett. **112**, 030602 (2014).

[10] S. Krishnamurthy, S. Ghosh, D. Chatterji, R. Ganapathy, and A. K. Sood, A micrometre-sized heat engine operating between bacterial reservoirs, Nat. Phys. **12**, 1134 (2016).

[11] R. Zakine, A. Solon, T. Gingrich, and F. van Wijland, Stochastic Stirling engine operating in contact with active baths, Entropy **19**, 193 (2017).

[12] J. S. Lee and H. Park, Carnot efficiency is reachable in an irreversible process, Sci. Rep. **7**, 10725 (2017).

[13] J. S. Lee, S. H. Lee, J. Um, and H. Park, Carnot efficiency and zero-entropy-production rate do not guarantee reversibility of a process, J. Korean Phys. Soc. **75**, 948 (2019).

[14] M. Polettini and M. Esposito, Carnot efficiency at divergent power output, Europhys. Lett. **118**, 40003 (2017).

[15] X.-L. Wu and A. Libchaber, Particle Diffusion in a Quasi-Two-Dimensional Bacterial Bath, Phys. Rev. Lett. **84**, 3017 (2000).

[16] K. C. Leptos, J. S. Guasto, J. P. Gollub, A. I. Pesci, and R. E. Goldstein, Dynamics of Enhanced Tracer Diffusion in Suspensions of Swimming Eukaryotic Microorganisms, Phys. Rev. Lett. **103**, 198103 (2009).

[17] H. Kurtuldu, J. S. Guasto, K. A. Johnson, and J. P. Gollub, Enhancement of biomixing by swimming algal cells in two-dimensional films, Proc. Natl. Acad. Sci. USA **108**, 10391 (2011).

[18] C. Maggi, M. Paoluzzi, N. Pellicciotta, A. Lepore, L. Angelani, and R. Di Leonardo, Generalized Energy Equipartition in Harmonic Oscillators Driven by Active Baths, Phys. Rev. Lett. **113**, 238303 (2014).

[19] C. Bechinger, R. Di Leonardo, H. Löwen, C. Reichhardt, G. Volpe, and G. Volpe, Active particles in complex and crowded environments, Rev. Mod. Phys. **88**, 045006 (2016).

[20] L. Dabelow, S. Bo, and R. Eichhorn, Irreversibility in Active Matter Systems: Fluctuation Theorem and Mutual Information, Phys. Rev. X **9**, 021009 (2019).

[21] N. Shiraishi, K. Saito, and H. Tasaki, Universal Trade-Off Relation Between Power and Efficiency for Heat Engines, Phys. Rev. Lett. **117**, 190601 (2016).

[22] A. Dechant and S.-I. Sasa, Entropic bounds on currents in Langevin systems, Phys. Rev. E **97**, 062101 (2018).

[23] P. Pietzonka and U. Seifert, Universal Trade-Off Between Power, Efficiency, and Constancy in Steady-State Heat Engines, Phys. Rev. Lett. **120**, 190602 (2018).

[24] F. L. Curzon and B. Ahlborn, Efficiency of a Carnot engine at maximum power output, Am. J. Phys. **43**, 22 (1975).

[25] F. Zamponi, F. Bonetto, L. F. Cugliandolo, and J. Kurchan, A fluctuation theorem for non-equilibrium relaxational systems driven by external forces, J. Stat. Mech. (2005) P09013.

[26] L. Caprini, U. M. B. Marconi, A. Puglisi, and A. Vulpiani, Comment on Entropy Production and Fluctuation Theorems for Active Matter, Phys. Rev. Lett. **121**, 139801 (2018).

[27] L. Caprini, U. M. B. Marconi, A. Puglisi, and A. Vulpiani, The entropy production of Ornstein-Uhlenbeck active particles: A path integral method for correlations, J. Stat. Mech. (2019) 053203.

[28] C. Kwon, J. Yeo, H. K. Lee, and H. Park, Unconventional entropy production in the presence of momentum-dependent forces, J. Korean Phys. Soc. **68**, 633 (2016).

[29] H. K. Lee, S. Lahiri, and H. Park, Nonequilibrium steady states in Langevin thermal systems, Phys. Rev. E **96**, 022134 (2017).

[30] T. Sagawa and M. Ueda, Fluctuation Theorems with Information Exchange: Role of Correlations in Stochastic Thermodynamics, Phys. Rev. Lett. **109**, 180602 (2012).

[31] A. Crisanti, A. Puglisi, and D. Villamaina, Nonequilibrium and information: The role of cross correlations, Phys. Rev. E **85**, 061127 (2012).

[32] J.-M. Park, H.-M. Chun, and J. D. Noh, Efficiency at maximum power and efficiency fluctuations in a linear Brownian heat-engine model, Phys. Rev. E **94**, 012127 (2016).

[33] C. Kwon, J. D. Noh, and H. Park, Nonequilibrium fluctuations for linear diffusion dynamics, Phys. Rev. E **83**, 061145 (2011).

[34] H.-M. Chun, L. P. Fischer, and U. Seifert, Effect of a magnetic field on the thermodynamic uncertainty relation, Phys. Rev. E **99**, 042128 (2019).

[35] R. Filliger and P. Reimann, Brownian Gyrator: A Minimal Heat Engine on the Nanoscale, Phys. Rev. Lett. **99**, 230602 (2007).

[36] K.-H. Chiang, C.-L. Lee, P.-Y. Lai, and Y.-F. Chen, Electrical autonomous Brownian gyrator, Phys. Rev. E **96**, 032123 (2017).

[37] H. Risken, *The Fokker-Planck Equation, Methods of Solution and Applications* (Springer, Berlin, 1996).

[38] É. Fodor, C. Nardini, M. E. Cates, J. Tailleur, P. Visco, and F. van Wijland, How Far from Equilibrium is Active Matter? Phys. Rev. Lett. **117**, 038103 (2016).

[39] U. M. B. Marconi, A. Puglisi, and C. Maggi, Heat, temperature and Clausius inequality in a model for active Brownian particles, Sci. Rep. **7**, 46496 (2017).

[40] D. Mandal, K. Klymko, and M. R. DeWeese, Entropy Production and Fluctuation Theorems for Active Matter, Phys. Rev. Lett. **119**, 258001 (2017).

[41] J. Thingna, D. Manzano, and J. Cao, Dynamical signatures of molecular symmetries in nonequilibrium quantum transport, Sci. Rep. **6**, 28027 (2016).

[42] J. Um, K. Dorfman, and H. Park, Coherence effect in a multilevel quantum-dot heat engine (unpublished).

[43] T. F. F. Farage, P. Krinninger, and J. M. Brader, Effective interactions in active Brownian suspensions, Phys. Rev. E **91**, 042310 (2015).

[44] H. Park, Entropy and thermodynamic second laws: New perspective—Stochastic thermodynamics and fluctuation theorems, J. Korean Phys. Soc. **72**, 1413 (2018).